NORSAR Scientific Report No. 1-2006

Semiannual Technical Summary

1 July - 31 December 2005

Frode Ringdal (ed.)

Kjeller, January 2006

6.2 Surface Wave Tomography for the Barents Sea and Surrounding Regions – Part II

6.2.1 Introduction

In a previous study (Part I; Levshin et al., 2005a) a new dataset of surface-wave observations from more than 150 local and regional events with travel paths through the greater Barents Sea region was compiled and group-velocity dispersion curves were measured for Love and Rayleigh waves in the period range 14 – 160 s. This large amount of new group-velocity measurements was used to enlarge the already existing data base compiled at the University of Colorado and to increase the path density in the region under investigation (Levshin *et al.*, 2001). This combined data set of group-velocity observations was inverted for 2D group-velocity maps (Barmin *et al.*, 2001; Ritzwoller *et al.*, 2002; Levshin *et al.*, 2005a). Pasyanos (2005) recently published another set of group-velocity maps for Eurasia and the European Artic, which show very similar large scale features in the greater Barents Sea region but which have far less resolution for smaller scale anomalies in that area.

As mentioned in Levshin *et al.* (2005a), it was planned to invert the new group velocity maps for Love and Rayleigh waves for a new 3D velocity model of the European Arctic. This paper summarizes the results of this inversion.

6.2.2 Inversion of the 3D tomographic S-velocity model

The 2D group-velocity maps derived from the new dataset of Love and Rayleigh wave group-velocity observations were the main input for a new 3D inversion for S-wave velocities. Due to the small number of short period surface-wave observations however, the resolution is limited for details in the structure of the crust, in particular in its upper most part. In addition, surface waves of higher frequencies are much more influenced by scattering at lateral heterogeneities in the crust.

To improve the inversion with respect to that, we applied a new crustal model of the Barents Sea and its surrounding areas, which had been derived in a joint project between the University of Oslo, NORSAR, and the USGS (Bungum *et al.*, 2005). This model with its detailed information on crustal thickness and sedimentary basins in the area helps to constrain the tomographic inversion based on surface wave data particularly in the shallow parts of the resulting model of crustal and upper mantle S-wave velocities.

Therefore, for the 3D inversion of the surface-wave data this crustal model was applied as an initial model. The upper crust with its information on sedimentary coverage of the greater Barents Sea region was used as constraint and not altered during the inversion. The lower crust and the Moho depth were also taken from the recent crustal model but this part of the model was also inverted for. Since the crustal model of Bungum *et al.* (2005) is a P-wave velocity model, the corresponding S velocities were calculated with the P-to-S velocity transformation as used in CRUST2.0 (Bassin *et al.*, 2000; http://mahi.ucsd.edu/Gabi/rem.dir/crust/crust2.html).

For the upper mantle part, the Colorado University (CU) model of Shapiro & Ritzwoller (2002) was used as initial model down to a depth of 250 km (see also http://ciei.colorado.edu/~nshapiro/MODEL/index.html). Below 300 km, we applied the Harvard model J362D28 (Antolik *et*

al., 2003) as input model. A smooth transition was used between these two models in the depth range from 250 to 300 km.

The 3D inversion method follows the technique described in detail by Shapiro & Ritzwoller (2002). The resulting 3D shear-velocity model of the crust and upper mantle beneath the European Arctic provides higher resolution and accuracy than previous models. In addition, the 3D S-velocity model was converted into a 3D P-velocity model using temperature-velocity relations for mantle material as described in Goes *et al.* (2000) and Shapiro & Ritzwoller (2004).

The inversion results are presented as deviations in shear-wave speed from the average S-wave speed in each layer of the model (in percent). Fig. 6.2.1 shows the new model in several horizontal slices in the range from 60 to 280 km depth. The new model reveals substantial variations in shear-wave speeds in the upper mantle across the region. Of particular note are clarified images of the mantle expression of first-order tectonic regimes like the mid-Atlantic ridge, the continental-ocean transition in the Norwegian Sea or a thickened crust beneath Novaya Zemlya (Fig. 6.2.2).

An extended region of increased velocity beneath the Barents Sea is dipping eastwards and suggests higher densities and thus an optional explanation for the evolution of the deep sedimentary basin in that region. This dipping structure is best seen along vertical profiles showing the velocity distribution over the entire modeled depth range. Fig. 6.2.2 presents four such profiles and in addition the velocity variations in 40 km depth, which reveal approximately the lateral change in the velocities relevant for Sn propagation. Engdahl & Schweitzer (2004a; 2004b) described pronounced differences in travel times and waveform shapes on NORSAR array recordings of nuclear explosions conducted both at the northern and at the southern nuclear test side on Novaya Zemlya. This observation may be explained by multipathing effects due to the dipping high velocity body.

6.2.3 Conclusions

The substantial data set of new surface group-velocity measurements combined with already existing data has provided the opportunity for constructing a new 3D shear-velocity model of the crust and upper mantle down to about 250 km beneath the European Arctic.

This model has higher spatial and depth resolution than previous models and clarifies or reveals important features of the tectonic setting in the region: continent-ocean boundary, a dipping slab-like high velocity zone in the upper mantle and the lithospheric structure under the deep sedimentary basin.

Ritzwoller *et al.* (2003) derived source specific travel-time corrections (SSSCs) based on 3D tomographic surface-wave model. The new 3D velocity model presented here may be used for refining these corrections for regional P and S waves propagating through the larger Barents Sea region.

Acknowledgements

For this study we requested and retrieved broadband and long periodic data from the Norwegian National Seismic Network (NNSN, University in Bergen), Kola Regional Seismological Center (KRSC, Apatity), Danmarks og Grønlands Geologiske Undersøgelse (GEUS, Copenhagen), Totalförsvarets forskningsinstitut (FOI, Stockholm), British Geological Service (BGS, Edinburgh), the Finish National Seismic Network (FNSN, University of Helsinki), and the international network operators and data centers IRIS and GEOFON. That they all made their data available for this study is gratefully acknowledged.

Anatol Levshin, University of Colorado
Johannes Schweitzer
Christian Weidle, University of Oslo
Nikolai Shapiro, University of Colorado
Nils Maercklin
Mike Ritzwoller, University of Colorado

References

Antolik, M., Y.J. Gu, A.M. Dziewonski & G. Ekström (2003). A new joint model of compressional and shear velocity in the mantle. *Geophys. J. Intl.* **153**, 443-466.

Barmin, M.P., M.H. Ritzwoller, & A.L. Levshin (2001). A fast and reliable method for surface wave tomography. *Pure Appl. Geophys.* **158**, 1351-1375.

Bassin, C., G. Laske, & G. Masters (2000). The current limits of resolution for surface wave tomography in North America. *EOS Trans. AGU* **81**(48), F879, Abstract S12A-03.

Bungum, H., O. Ritzmann, N. Maercklin, J.I. Faleide, W.D. Mooney, & S.T. Detweiler (2005). Three-dimensional model for the crust and upper mantle in the Barents Sea region. *EOS Trans. AGU* **86**, 160-161.

Engdahl, E.R. & J. Schweitzer (2004a). Observed and predicted travel times of Pn and P phases recorded at NORSAR from regional events. In: Semiannual Technical Summary, 1 January – 30 June 2004, *NORSAR Scientific Report* **2-2004**, 51-56.

Engdahl, E.R. & J. Schweitzer (2004b). Observed and predicted travel times of Pn and P phases recorded at NORSAR from regional events. *Eos Trans. AGU* **85** (47), Abstract S13B-1050.

Goes, S., R. Govers & R. Vacher (2000). Shallow mantle temperatures under Europe from P and S wave tomography. *J. Geophys. Res.* **105**, 11,153-11,169.

Levshin, A.L., M.H. Ritzwoller, M.P. Barmin, A. Villaseñor & C.A. Padgett (2001). New constraints on the Arctic crust and uppermost mantle: surface wave group velocities, P_n, and S_n. *Phys. Earth Planet. Int.* **123**, 185-204.

Levshin, A., Ch. Weidle & J. Schweitzer (2005a). Surface wave tomography for the Barents Sea and surrounding regions. In: Semiannual Technical Summary, 1 January – 30 June 2005, *NORSAR Scientific Report* **2-2005**, 37-48.

Levshin, A., J. Schweitzer, Ch. Weidle, N. Maercklin, N. Shapiro & M. Ritzwoller (2005b). Surface wave tomography of the European Artic, *Eos Trans. AGU* **86 (52)**, Fall Meeting Supplement, Abstract S51E-1053.

Pasyanos, M.E. (2005). A variable resolution surface wave dispersion study of Eurasia, North Africa, and surrounding regions. *J. Geoph. Res.* **110**, B12301, doi:10.1029/2005JB003749, 22 pp.

Ritzwoller M.H., N.M. Shapiro, M.P. Barmin & A.L. Levshin (2002). Global surface wave diffraction tomography. J. Geoph. 107(B12), 2335, ESE 4-1 – 4-13, doi:10.1029/2002JB001777.

Ritzwoller, M.H., N.M. Shapiro, A.L. Levshin, E.A. Bergman & E.R. Engdahl (2003). The ability of a global 3-D model to locate regional events. *J. Geophys. Res.* **108**(B7), 2353, ESE 9-1 – 9-24.

Shapiro, N.M. & M.H. Ritzwoller (2002). Monte-Carlo inversion for a global shear velocity model of the crust and upper mantle. *Geophys. J. Int.* **151**, 88-105.

Shapiro, N.M. & M.H. Ritzwoller (2004). Thermodynamic constraints on seismic inversions. *Geophys. J. Int.* **157**, 1175-1188, doi:10.1111/j.l365-246X.2004.02254.x.

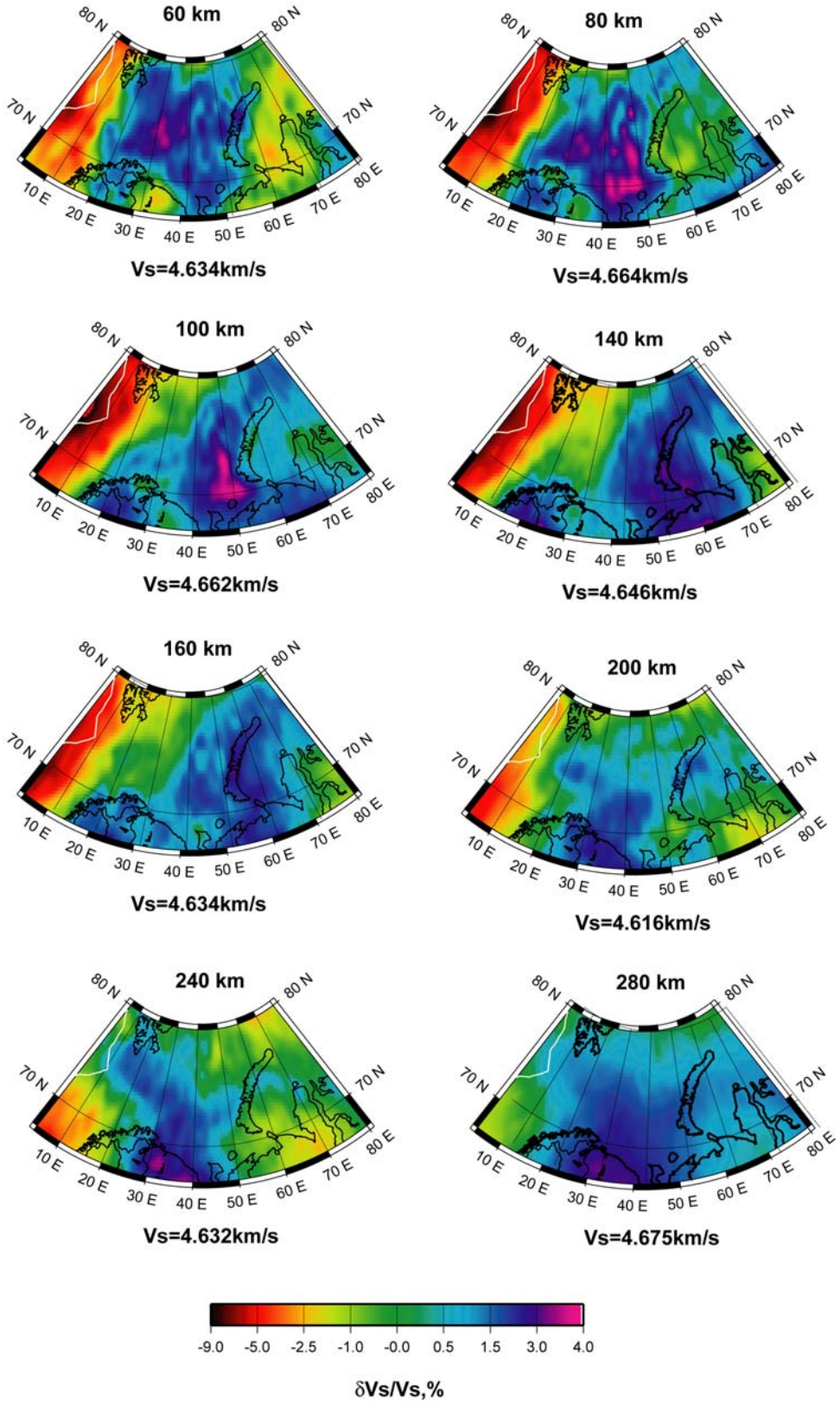

Fig. 6.2.1. Results of the 3D tomographic inversion, shear wave velocities in percentage relative to the average velocity; shown are the S velocities in different depths. The mean S velocity is given for each map separately.

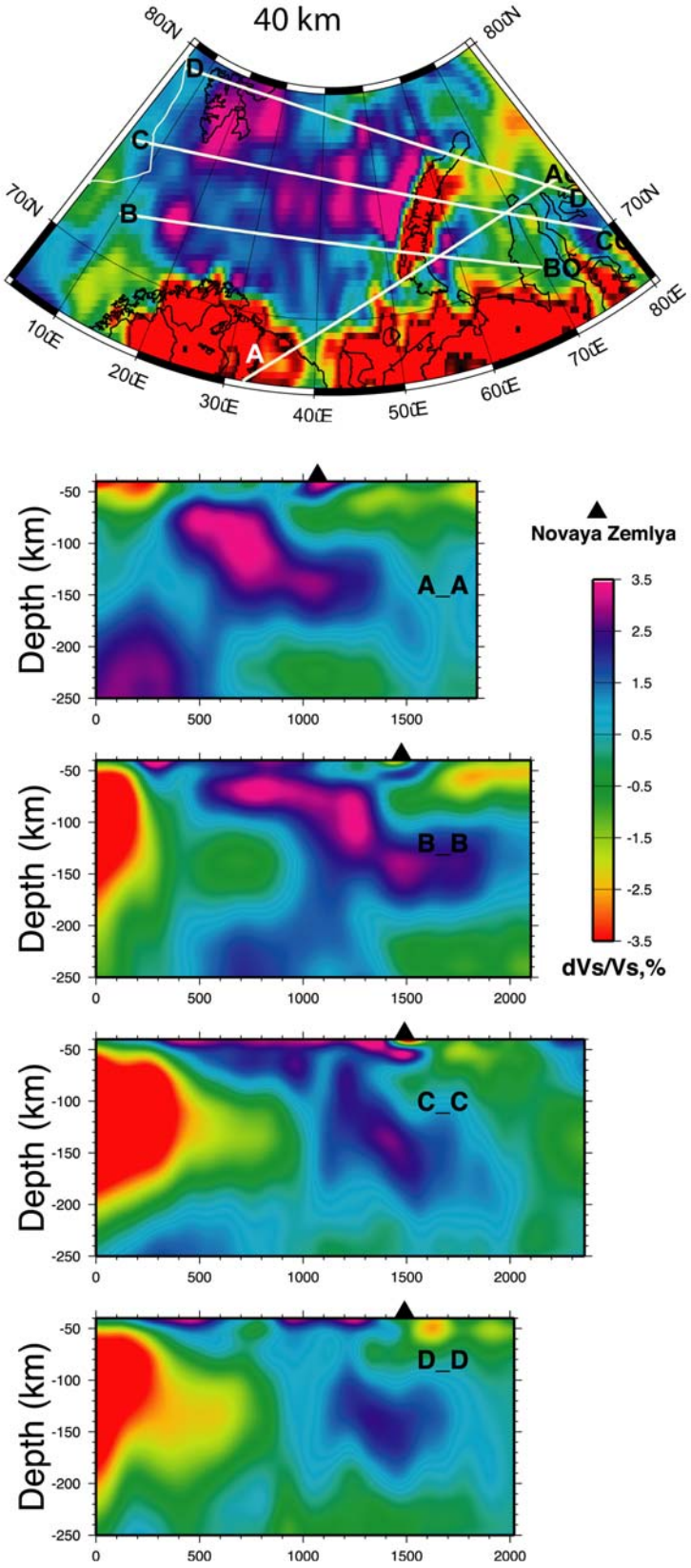

Fig. 6.2.2. On top are shown the relative S velocities in 40 km depth with respect to the mean velocity and the location of four transects. The four lower figures show the S-velocity perturbations along these transects.